Modeling Ca^{2+} Dynamics of Mouse Cardiac Cells Points to a Critical Role of SERCA's Affinity for Ca^{2+}

Luc Raeymaekers,* Ilse Vandecaetsbeek, Frank Wuytack, and Peter Vangheluwe
Laboratory of Cellular Transport Systems, Department of Molecular Cell Biology, Katholieke Universiteit Leuven, Campus Gasthuisberg, Leuven, Belgium

ABSTRACT The SERCA2a isoform of the sarco/endoplasmic reticulum Ca^{2+} pumps is specifically expressed in the heart, whereas SERCA2b is the ubiquitously expressed variant. It has been shown previously that replacement of SERCA2a by SERCA2b in mice ($SERCA2^{b/b}$ mice) results in only a moderate functional impairment, whereas SERCA activity is decreased by a 40% lower SERCA protein expression and by increased inhibition by phospholamban. To find out whether the documented kinetic differences in SERCA2b relative to SERCA2a (i.e., a twofold higher apparent Ca^{2+} affinity, but twofold lower maximal turnover rate) can explain these compensatory changes, we simulated Ca^{2+} dynamics in mouse ventricular myocytes. The model shows that the relative Ca^{2+} transport capacity of SERCA2a and SERCA2b depends on the SERCA concentration. The simulations point to a dominant effect of SERCA2b's higher Ca^{2+} affinity over its lower maximal turnover rate. The results suggest that increased systolic and decreased diastolic Ca^{2+} levels in unstimulated conditions could contribute to the downregulation of SERCA in $SERCA2^{b/b}$ mice. In stress conditions, Ca^{2+} handling is less efficient by SERCA2b than by SERCA2a, which might contribute to the observed hypertrophy in $SERCA2^{b/b}$ mice. Altogether, SERCA2a might be a better compromise between performance in basal conditions and performance during β-adrenergic stress.

INTRODUCTION

The transient release of Ca^{2+} from the sarcoplasmic reticulum (SR) couples activation to contraction in skeletal and cardiac muscle. The state of filling of the SR with Ca^{2+} is thus an important factor in determining contractile strength. Ca^{2+} loading of the SR is catalyzed by SERCA Ca^{2+}-transport ATPases, which pump Ca^{2+} back into the SR after its release, thereby contributing for ~50–90% to the termination of the Ca^{2+} transient in mammalian ventricular myocytes (1). In addition, SERCA-mediated Ca^{2+} transport plays a central role in the β-adrenergic regulation of the heart via interaction with the accessory membrane protein phospholamban (2). Phosphorylation of phospholamban during β-adrenergic stress releases its inhibitory interaction, resulting in faster relaxation, augmented loading of the SR with Ca^{2+}, and stronger contraction. Alterations in SERCA's Ca^{2+} pumping activity also play a central role in heart pathology. A decline in the Ca^{2+} load of the SR caused by decreased affinity of SERCA for Ca^{2+} or by decreased SERCA levels is often associated with heart failure, whereas Ca^{2+} overload of the SR can cause arrhythmia (3–6).

Although in the heart, slow skeletal muscle, and to some extent smooth muscle, express the SERCA2a splice variant, all other cell types predominantly make use of SERCA2b, which is considered the housekeeping isoform. This differential distribution suggests that SERCA2a is better adapted to function in cells like striated muscle cells, which generate faster Ca^{2+} transients than most other cell types. This raises the question of the functional link between the characteristics of cellular Ca^{2+} dynamics and those of the reticular Ca^{2+} pumps. SERCA2b differs functionally from SERCA2a in its twofold higher affinity for cytosolic Ca^{2+} and its approximately twofold lower maximal turnover rate (7,8). The physiological meaning of these characteristics was explored in the $SERCA2^{b/b}$ mouse model. In these genetically modified mice, the formation of the SERCA2a splice variant is prevented and splicing to the default SERCA2b form is favored. A remarkable finding is that these interventions result in a drop of the SERCA levels to ~60% of wild-type. Moreover, expression of the SERCA inhibitory protein phospholamban is increased, and phosphorylation of phospholamban, which removes the protein's inhibitory effect on SERCA, is decreased (9). Although the animals develop cardiac hypertrophy, Ca^{2+} transients in isolated ventricular cells appear normal except when challenged with higher Ca^{2+} loads (10). Altogether, this phenotype suggests that in the mouse heart, the higher affinity of SERCA2b for Ca^{2+} represents a more critical parameter than its lower maximal speed. An increased activity of the SERCA pump below 0.1 μM concentration of cytosolic Ca^{2+} is apparently not well tolerated in the heart, resulting in downregulation of SERCA expression and upregulation of inhibitory phospholamban. This interpretation is further supported by various crosses of the $SERCA2^{b/b}$ mice with SERCA2b transgenes. Inducing a further increase of the Ca^{2+} affinity by crossing with phospholamban knockout animals results in further downregulation of the SERCA2b level to about one-third of the wild-type without severely impacting basal Ca^{2+} handling (11). Conversely, enforced expression of

Submitted June 3, 2010, and accepted for publication January 14, 2011.

*Correspondence: Luc.Raeymaekers@med.kuleuven.be

Editor: David A. Eisner.

0006-3495/11/03/1216/10 $2.00

doi: 10.1016/j.bpj.2011.01.024

SERCA2b obtained in crosses with SERCA2b transgenes was compensated by an increased inhibition by phospholamban (12).

To better understand the consequences of the enforced SERCA2a-to-SERCA2b switch in mouse cardiac myocytes, we designed a computer model of the intervention that takes into consideration the presently known kinetic differences between the two isoforms. This model includes information about differences in rate constants of specific substeps of the SERCA2 catalytic cycle.

METHODS

Simulation of SERCA2a and SERCA2b activity

The different kinetic properties of Ca^{2+} transport by SERCA2a and SERCA2b have been well documented (7,8,11,13). SERCA2b differs from SERCA2a in its nearly twofold lower maximal turnover rate, its approximately twofold higher affinity for cytosolic Ca^{2+} and the lower sensitivity of its maximal turnover rate to inhibition by luminal Ca^{2+} ($[Ca^{2+}]_{SR}$). In addition, Dode et al. (7) have identified different kinetics of several specific partial reaction steps. Using the seven-step Post-Albers-type schema (Fig. 1 *A*; the multistep scheme), the changes reside in steps 3, 4, and 7, which were modified accordingly in the SERCA2b scheme (Table S1 in the Supporting Material). Fig. 1 *B* shows the Ca^{2+} dependence of the steady-state turnover rate of SERCA2a and SERCA2b, with $[Ca^{2+}]_{SR}$ set equal to $[Ca^{2+}]_{cyt}$. To obtain a sufficient shift of the Ca^{2+} affinity, r_2 was assigned a smaller value also, in accordance with recent structural data suggesting a stabilization of E1Ca or E1 or both (13). These documented modifications represent a stronger decrease of reverse compared to forward rate constants, predicting that SERCA2b is able to build a steeper Ca^{2+} gradient over the SR membrane (Fig. S1). However, the kinetic scheme predicts that at lower $[Ca^{2+}]_{SR}$ that moderately decrease SERCA activity, SERCA2b is more easily inhibited due to the lower value of k_7 (Fig. S2). This property makes it more difficult to model the experimental data on the $SERCA2^{b/b}$ mouse, which suggest a higher over-all Ca^{2+} transport rate for SERCA2b. It is possible that other unidentified differences exist in SERCA2b at the level of the luminal Ca^{2+}-binding sites that alleviate this higher sensitivity to inhibition by luminal Ca^{2+}, but such hypothetical modifications were not tested.

In addition to the seven-step Post-Albers-type cycle, we also used a single equation to represent SERCA activity (denoted as the one-step scheme) that captures the transport rate of the multistep scheme under conditions of constant $[Ca^{2+}]_{cyt}$ and nonjunctional SR calcium concentration ($[Ca^{2+}]_{NSR}$) (see Supporting Material).

In ventricular myocytes, the SERCA level differs between animal species and correlates with the heart rate in mammals (1). In the faster-beating heart of small animals like rats (~350 beats/min), it can reach up to 50 μmol/kg (14). In mice (600 beats/min), the SERCA level required to account for the relaxation rate is even higher. In our models, and with a V_{max} of ~30 s^{-1}, a SERCA2a concentration of several tens of μM/liter cell volume was required to obtain proper relaxation rates (see Results).

Whole-cell Ca^{2+} dynamics model with a homogeneous cytosolic compartment (cell model)

This simple model considers two cellular compartments, the SR, with a Ca^{2+} pump and a Ca^{2+}-release channel, and the cytosol (Fig. 2 *A*). SR and cytosol are both treated as homogeneous. Ca^{2+} binding to calsequestrin in the SR is instantaneous. Ca^{2+} binding to troponin C (*TRPN*) is described by

$$\frac{d[TRPNCa]}{dt} = [TRPN_{total} - TRPNCa] \times [Ca^{2+}]_{cyt} \times kt_{on} - [TRPNCa] \times kt_{off}. \quad (1)$$

Two different values were used for the off-rate constant of the Ca-troponin complex to obtain sufficiently strong binding to troponin during systole (kt_{offsys}, 25 s^{-1}) and sufficiently fast unbinding during diastole (kt_{offdia}, 50 s^{-1}). An increase of kt_{off} during the shortening phase of the heartbeat is in accordance with physiological data and is known as shortening deactivation (see Edman (15) and Hinken and Solaro (16) for review). The transitions between both kt_{off} values occurred linearly with time, between 20 and 60 ms (kt_{offsys} to kt_{offdia}), and between 60 ms and the end of the beat (kt_{offdia} to kt_{offsys}).

Since this model is only used to illustrate the implications of the SERCA model on Ca^{2+} dynamics during a single beat, Ca^{2+} influx and efflux are omitted. Parameters are given in Table S2.

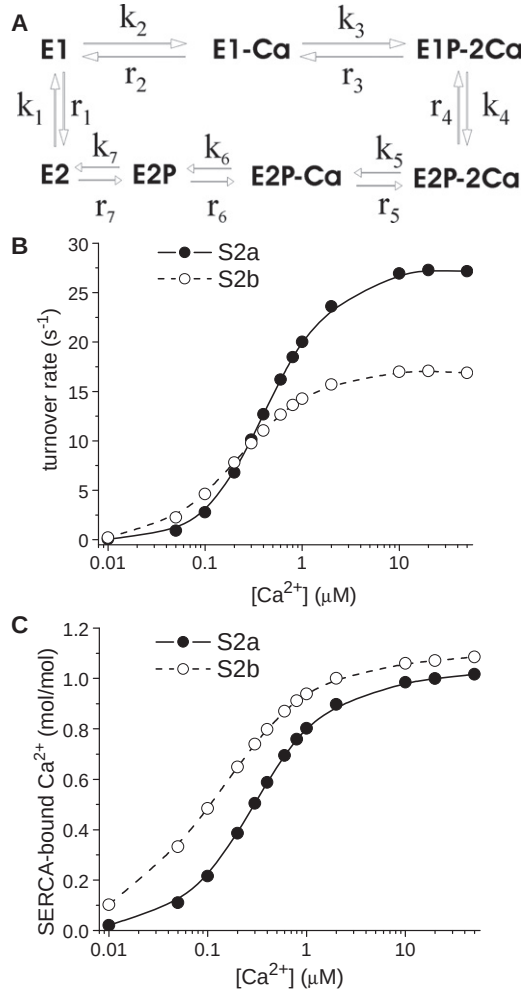

FIGURE 1 Reaction scheme of the SERCA pump and its equilibrium behavior. (*A*) Seven-step Post-Albers-type reaction scheme of the SERCA pump. (*B*) Ca^{2+}-activation curves of SERCA2a and SERCA2b obtained from the seven-step SERCA model using the rate constants from Table S1. S2a, SERCA2a; S2b, SERCA2b. (*C*) Dependence of the amount of SERCA-bound Ca^{2+} on Ca^{2+} concentration.

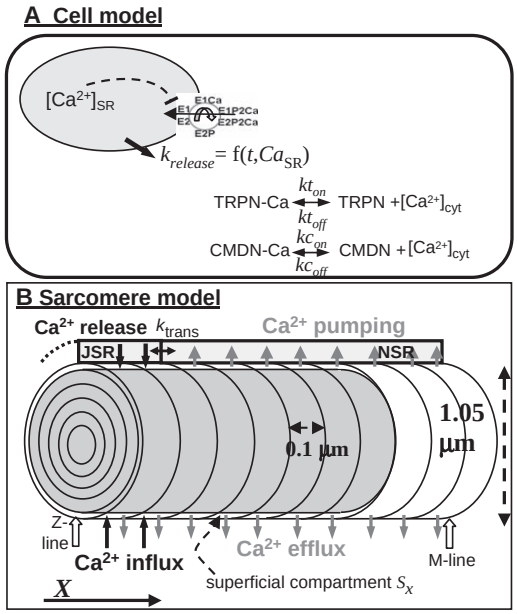

FIGURE 2 Outline of the models used in the simulations. (*A*) The cell model. The cytosol is considered as a homogeneous compartment. Since this model is used only to simulate one isolated Ca^{2+} transient, Ca^{2+} influx and efflux are omitted. (*B*) Geometry of a half-sarcomere in the sarcomere model (not to scale). The region between the Z- and M-disks is divided into five concentric compartments of 0.1-μm thickness surrounded by a contractile filament-free sheet of 0.25 μm. The longitudinal direction is divided into 10 compartments of 0.1 μm each, all of which contain calmodulin and ATP and seven of which contain troponin C (*shaded region*). Ca^{2+} is released from the JSR into the two peripheral volumes closest to the Z-disk. SERCAs translocate Ca^{2+} from the outer compartments of segments 3–10 into the nonjunctional SR (NSR). Ca^{2+} efflux occurs from all peripheral compartments.

The rate of change of the Ca^{2+} concentration of the cytosolic compartment due to activity of the SERCA multistep scheme is calculated according to

$$\frac{d[\mathrm{Ca}^{+}]_{\mathrm{cyt}}}{dt} = -\big([E1] \times [\mathrm{Ca}^{2+}]_{\mathrm{cyt}} \times k_2 + [E1Ca] \times [\mathrm{Ca}^{2+}]_{\mathrm{cyt}} \times k_3 - [E1Ca] \times r_2 - [E1P2Ca] \times r_3\big). \quad (2)$$

The rate of change of the free Ca^{2+} concentration in the SR induced by the SERCA multistep scheme is represented by

$$\frac{d[\mathrm{Ca}]_{\mathrm{SR}}}{dt} = \frac{\big(-[E2P] \times [\mathrm{Ca}^{2+}]_{\mathrm{SR}} \times r_6 - [E2PCa] \times [\mathrm{Ca}^{2+}]_{\mathrm{SR}} \times r_5 + [E2P2Ca] \times k_5 + [E2PCa] \times k_6\big) \times \frac{Vol_{\mathrm{cyt}}}{Vol_{\mathrm{SR}}}}{1 + \frac{CSQN\mathrm{max} * CSQNK_d}{\left(1 + \frac{CSQNK_{0.5}}{[\mathrm{Ca}^{2+}]_{\mathrm{SR}}}\right)^2 \times [\mathrm{Ca}^{2+}]_{\mathrm{SR}}}}. \quad (3)$$

*CSQN*max represents the maximum Ca^{2+}-binding capacity of the SR and $CSQNK_d$ the dissociation constant for luminal Ca^{2+} binding.

When using the one-step SERCA representation, Eq. 2 and the Ca^{2+} flux part of Eq. 3 were replaced by the appropriate relations, as described in the previous section.

Changes of Ca^{2+} concentrations due to Ca^{2+} release from the SR are given by

$$\frac{d[\mathrm{Ca}^{2+}]_{\mathrm{SR}}}{dt} = -k_{release}\big([\mathrm{Ca}]_{\mathrm{JSR}} - [\mathrm{Ca}]_{\mathrm{cyt}}\big) = \frac{d[\mathrm{Ca}^{2+}]_{\mathrm{cyt}}}{dt}\frac{Vol_{\mathrm{SR}}}{Vol_{\mathrm{cyt}}}. \quad (4)$$

The rate constant $k_{release}$ depends on time. $k_{release}$ rises linearly with time during 5 ms, from zero to a peak value (k_{relMax}) of 180 s^{-1}, and then decreases linearly to zero, also in 5 ms.

The compartmentalized sarcomere model (sarcomere model)

The geometry and position of the various Ca^{2+} fluxes are indicated in Fig. 2 *B*. The SR is considered continuous around the myofibril, preserving symmetry and reducing computation time (17). Parameter values are given in Table S3. Parameters and computations are the same as for the cell model, except for the additional elements given below. The program is run until a stable state is reached, defined as a $<10^{-4}$% change of the maximal level of troponin-bound Ca^{2+} between two consecutive beats.

To obtain a reasonable fast rate of Ca^{2+} diffusion, binding of Ca^{2+} to ATP and simultaneous diffusion of Ca^{2+}-ATP were included (18). The flux due to diffusion between two compartments is calculated from the diffusion coefficient (D), the contact area (A), the concentration difference (ΔC) and the distance separating the centers of the compartments (Δx) by a numerical approximation of Fick's law:

$$Flux = -A \times D \times \Delta C/\Delta x. \quad (5)$$

Ca^{2+} influx lasts for the first 10 ms of the beat, is constant with time, and is inhibited by the calcium concentration in the junctional SR ($[Ca^{2+}]_{JSR}$) according to

$$Influx = \frac{InflMax}{1 + \left(\frac{[\mathrm{Ca}^{2+}]_{\mathrm{JSR}}}{0.5}\right)^{1.5}}. \quad (6)$$

(concentrations in mM). Maximal Ca^{2+} influx, *InflMax*, is set at a value such that it accounts for ~10% of the total Ca^{2+} entering the sarcomere during regular pacing at 9 Hz in unstimulated conditions, as observed in cardiac cells of small mammals (1). In addition to this activating Ca^{2+} influx, there is a continuous background influx in longitudinal segments 1–7 amounting to 7.2 μM s^{-1} in total.

The rate of Ca^{2+} efflux depends on the free Ca^{2+} concentration in the superficial subcompartment S_x ($[Ca]_{Sx}$) according to

$$\frac{d[Ca]_{Sx}}{dt} = -\frac{(EV)_{\max}}{1 + \left(\frac{(EK)_{0.5}}{[\mathrm{Ca}]_{cSx}}\right)}. \quad (7)$$

Since Ca^{2+} efflux mainly occurs via the Na^+/Ca^{2+} exchanger, which starts to operate in the forward mode only at a sufficiently polarized membrane potential, Ca^{2+} efflux was switched off during the initial period of each beat, set at 12 ms.

For convenience, an apparent rate constant of Ca^{2+} release was used that applies to the change of the total JSR Ca^{2+} content instead of $[Ca^{2+}]_{JSR}$. This apparent rate constant, $k_{release}$, depends on time and increases with increasing $[Ca^{2+}]_{JSR}$ to simulate the potentiating effect of SR Ca^{2+} load on the release (19). The time-dependent component ($k_{release,time}$) rises linearly with time during 5 ms from zero to a peak value (k_{relMax}) of 6600 L s^{-1} and then decreases linearly to zero, also in 5 ms. k_{relMax} corresponds to a rate constant of 450 s^{-1} at a $[Ca^{2+}]_{JSR}$ of 0.5 mM. $k_{release}$ is given by (concentrations in mM)

$$k_{release} = k_{release,time}\frac{1}{\left(1+\frac{0.5}{[Ca]_{JSR}}\right)}, \quad (8)$$

The maximum rate constant of Ca^{2+} leak from the JSR and NSR was set at 0.33 L s^{-1} and dependent on $[Ca^{2+}]_{JSR}$ as in Eq. 8.

The change of the Ca^{2+} concentration in the peripheral compartments and in the NSR due to SERCA activity was calculated either as a single-state SERCA representation or as a multistate SERCA scheme.

Transfer of Ca^{2+} between the JSR and NSR is governed by the rate constant k_{trans}:

$$\frac{d[Ca]_{JSR}}{dt} = -k_{trans}\left([Ca]_{JSR}-[Ca]_{NSR}\right) = -\frac{d[Ca]_{NSR}}{dt}\frac{Vol_{JSR}}{Vol_{NSR}}. \quad (9)$$

The models were programmed in Delphi (Borland Software, Austin, TX) using the basic Euler method and run with constant time steps of 0.001 ms. To exclude possible errors arising from the discreteness of the time steps that may artifactually induce differences between models incorporating SERCA2a or SERCA2b, results were compared between runs with and runs without bookkeeping of total Ca^{2+} of the system, based on the integrated amount of Ca^{2+} influx and Ca^{2+} efflux. When the program was run with regular pacing until steady state (typically 100–300 beats), diastolic and peak systolic levels of troponin-bound Ca^{2+} differed at most by ~0.03%. These small values demonstrate that the effect of various SERCA kinetic schemes cannot be explained by the accumulation of computing errors.

RESULTS

The effect of various SERCA representations on myofilament activation during a single beat in the cell model

Ca^{2+} binds not only to troponin C, determining the degree of myofilament contraction, but also to SERCA before its complete translocation across the SR membrane. Thus, troponin C and SERCA compete for Ca^{2+} binding, influencing the amount of Ca^{2+} available for contraction. Multistate schemes take this into account and predict a faster rate of Ca^{2+} removal from the cytosol in the early phase of the Ca^{2+} transient than does the one-step Hill-type equation. Consequently, in such a model, a smaller fraction of all Ca^{2+} that enters the sarcomere will bind to the contractile filaments, predicting a reduced contraction. The implications for a single isolated Ca^{2+} transient, starting from the same initial conditions ($[Ca^{2+}]_{cyt}$ = 0.08 μM, $[Ca^{2+}]_{SR}$ = 0.5 mM), are shown in Fig. 3 for a model that considers the cytosol as a homogeneous compartment (cell model). The amount of Ca^{2+} release was adjusted such that it caused a peak level of ~60% average saturation of troponin at a SERCA concentration of 40 μM using the SERCA2a multistep scheme. This value corresponds to 26 μM troponin-bound Ca^{2+} above the diastolic level (assuming 0.1 μM free Ca^{2+}), close to the accepted value of ~27 μM for rabbit myocytes (3). With the one-step SERCA2a models, a much higher peak level of troponin-bound Ca^{2+} is reached (42.2 μM compared to 28.2 μM (Table 1)). The calculated amount of Ca^{2+} that rapidly binds to SERCA also differs between SERCA2a and SERCA2b (Fig. 3 and Table 1). For example, at peak levels of calcium saturation, 48.7% of all Ca^{2+} released is bound to SERCA2a (multistep) compared to 43.3% for SERCA2b. This difference can be explained by differences in kinetics of Ca^{2+} binding during the rising phase of the Ca^{2+} transient and by the difference in steady-state Ca^{2+} affinity: as is clear from Fig. 1 *C*, additional Ca^{2+} binding by SERCA2b above that by SERCA2a is higher at low Ca^{2+} levels than at high concentrations, leaving less room for extra Ca^{2+} binding during systole.

The simulations above show that the time course of the changes of $[Ca^{2+}]_{cyt}$ at the level of troponin C relative to that near the SERCA pumps may have implications for the effects of the SERCA2a-to SERCA2b switch.

Ca^{2+} transients during a single beat in the sarcomere model

To more faithfully reproduce the time course of the Ca^{2+} concentration changes near the Ca^{2+} pumps, we used the sarcomere model, which takes into account diffusion delays between the Ca^{2+} release sites, the cytosolic Ca^{2+} buffers, and the SR.

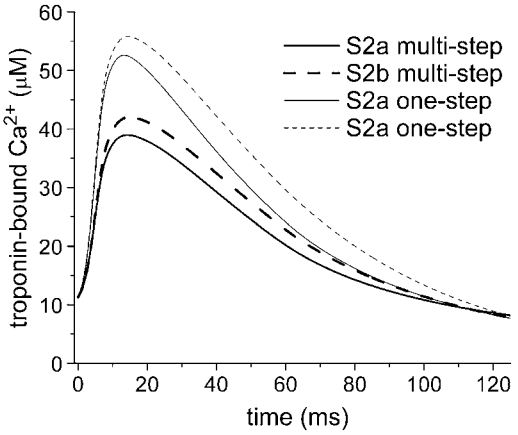

FIGURE 3 Simulation of a single beat in the cell model. Various SERCA schemes result in different peak values of troponin-bound Ca^{2+} transients.

TABLE 1 Systolic Ca^{2+} pools (one single beat)

	Multistep		One-step	
	S2a	S2b	S2a	S2b
ΔPeak Ca-troponin (μM)				
Cell model	28.2	31.1	42.2	45.0
Sarcomere model	27.6	28.8	35.0	37.4
ΔPeak Ca-SERCA (μM)				
Cell model	26.8	23.8		
Sarcomere model	19.8	18.4		
SERCA-bound Ca, % of total				
Cell model	48.7	43.3		
Sarcomere model	41.8	39.0		

Distribution of bound Ca^{2+} over troponin and SERCA at the peak systolic level during a single isolated beat starting from identical initial conditions ($[Ca^{2+}]_{cyt} = 0.08$ μM, $[Ca^{2+}]_{SR} = 0.5$ mM), compared between the cell and sarcomere models and between SERCA2a and SERCA2b. Troponin-bound Ca^{2+} and SERCA-bound Ca^{2+} are represented as the difference between systolic and diastolic levels (Δ*Peak*) in absolute concentration, and for SERCA-bound Ca^{2+} also as the percentage of total bound Ca^{2+}.

Fig. 4 *A* shows the temporal and spatial distribution of troponin-bound Ca^{2+} during a single beat in the sarcomere model incorporating SERCA2a. Ca^{2+} is rapidly bound to troponin in the segments close to the Z-disk. In the more central segments of the sarcomere, there is a short delay and the peak level is considerably lower. In cardiac muscle, intrasarcomeric Ca^{2+} gradients can be expected to be higher than in fast skeletal muscle, because in the latter, Ca^{2+} is released at sites located closer to the center of the sarcomere. Significant Ca^{2+} gradients within sarcomeres of cardiac cells have also been observed experimentally (20).

Troponin-bound Ca^{2+} of the transient shown in Fig. 4 *A* averaged over the whole sarcomere is shown in Fig. 4 *B* (*solid line*). This transient started from the same initial conditions as the transient in the cell model in the previous section (Fig. 3), and with a similar amplitude. As in the cell model, the peak level of troponin-bound Ca^{2+} in the sarcomere model differs between multistep and one-step SERCA schemes and between SERCA2a and SERCA2b. However, the differences are smaller compared to the cell model (Table 1), which can be explained by a relatively slower rise of Ca^{2+} close to the SERCA pumps. Compared to the cell model, the difference in the peak troponin-bound Ca^{2+} between the SERCA2a multistep and one-step schemes was reduced from 42.2 − 28.2 = 14 to 35 − 27.6 = 7.4 μM. The difference caused by the SERCA2a-to-SERCA2b switch was reduced from 4.9 (33.1 − 28.2 μM) to 1.2 μM (28.8 − 27.6). Also, the fraction of the released Ca^{2+} that rapidly binds to SERCA2a (represented as the multistep scheme) is reduced from 48.7% to 41.8%. The respective values for SERCA2b were 43.3 and 39% (Table 1). Thus, the sarcomere model favors Ca^{2+} binding to troponin by reducing the time of diffusion of Ca^{2+} toward the filaments relative to that toward the SR, which results in less futile Ca^{2+} cycling.

In the initial phase of the Ca^{2+} reuptake, Ca^{2+} rise in the SR lumen is about equally fast for SERCA2a and SERCA2b (Fig. 4 *C*), which points to the lower V_{max} of SERCA2b having a less significant role than expected. In the later phase, when $[Ca^{2+}]_{cyt}$ is low, Ca^{2+} transport by SERCA2b is slightly faster due to its higher Ca^{2+} affinity, resulting in an overall higher total Ca^{2+}-transport activity. With SERCA2b, a high level of troponin-bound Ca^{2+} is maintained for a longer time, thus prolonging contraction (early phase). However, this prolonged activation occurs with preservation of low diastolic levels, even below control levels (later phase) (Fig. 4 *B*). This is further illustrated in Fig. 4 *E*, which shows the time-integrated amount of Ca^{2+} removed from the cytosol, that is, the sum of Ca^{2+} translocated across the SR membrane into the lumen and Ca^{2+} bound to SERCA that is in surplus of the end-diastolic level. Ca^{2+} buffering by the multistep SERCA schemes is visible as the fast rise in the initial phase of the beat, which is slightly faster for SERCA2a than for SERCA2b (see also Fig. 4 *D*). The curves clearly show the faster Ca^{2+} translocation by SERCA2b in the later phase of the Ca^{2+} transient. This difference becomes more clear with time after the stimulus, resulting in a higher SR Ca^{2+} load in a resting cell (Fig. S3). Thus, these simulations show that in a single beat, Ca^{2+} availability for contraction could be more efficient in the presence of SERCA2b than in the presence of SERCA2a, an unexpected finding.

It should be noted that the differences in the amplitude of the Ca^{2+} transient caused by the SERCA2a-to-SERCA2b switch in the multistep and one-step schemes should be attributed to different, although somewhat related, explanations: the enhanced transient in the presence of SERCA2b is due to the lower V_{max} in the one-step model, whereas it is mainly caused by the lower Ca^{2+} buffering in the multistep scheme.

Ca^{2+} transients of the sarcomere model during regular pacing

To test whether the previous observations are also valid in conditions of regular pacing, the sarcomere model was run at specific stimulation frequencies till the output was stable. In a first set of simulations, the SERCA concentration was varied (Fig. 5). Changing the SERCA level between 20 and 100 μM has a relatively mild effect, especially on the peak level of troponin-bound Ca^{2+}, demonstrating a strong autoregulatory effect. This result can be explained by the observation that decreased Ca^{2+} buffering by the pump compensates for the decreased Ca^{2+} transport. In line with this interpretation, the replacement of SERCA2a by SERCA2b, the latter presenting less Ca^{2+}-buffering capacity, causes a higher peak level, and this increase is more pronounced with increasing SERCA concentration.

Transients of troponin-bound Ca^{2+} at 8 Hz pacing and the effect of equimolar replacement of SERCA2a by SERCA2b

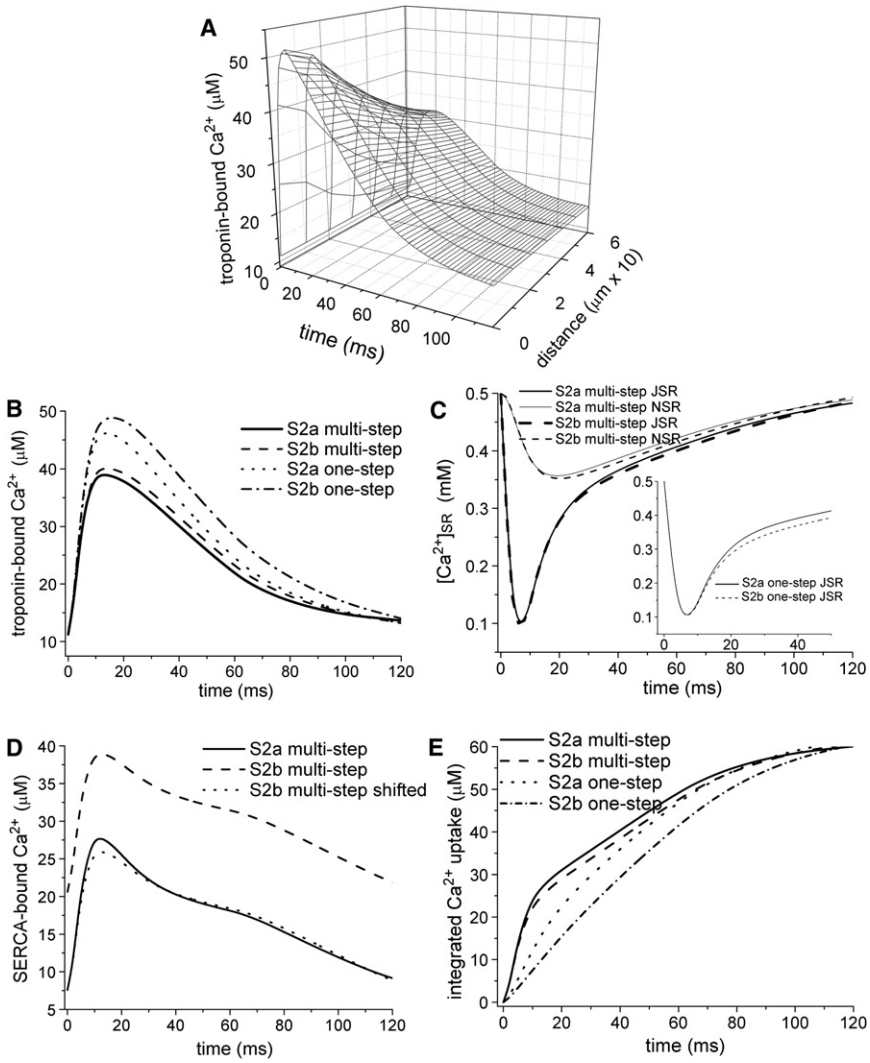

FIGURE 4 Examples of the dynamics of a single beat in the sarcomere model. (*A*) Change of troponin-bound Ca^{2+} in space and time in the presence of SERCA2a. In each segment in the *x* direction (distance from Z-disk (Fig. 2 *B*)), the concentration of troponin-bound Ca^{2+} was averaged over the five concentric rings subdividing the segment. (*B*) Time course of troponin-bound Ca^{2+} averaged over the whole sarcomere, using the SERCA multistep or one-step representation. (*C*) Time course of the luminal Ca^{2+} concentration in the JSR and NSR in the presence of SERCA2a or SERCA2b. (*Inset*) Initial phase for the SERCA one-step equations. (*D*) Time course of the change of SERCA-bound Ca^{2+}. The dotted line shows Ca^{2+} bound to SERCA2b shifted down to the same level as SERCA2a (*solid line*) at time zero. (*E*) Integrated amount of Ca^{2+} removed from the cytosol by various SERCA schemes starting from the initiation of the Ca^{2+} transient at time zero.

are shown in Fig. 6 *A*. As in the simulations of one single transient, the peak amplitude is slightly enhanced by the isoform switch, and the Ca^{2+}-bound state of troponin is prolonged. The enhanced amplitude cannot be explained by an increased loading of the SR with Ca^{2+}, because $[Ca^{2+}]_{SR}$ is slightly lower with SERCA2b (Fig. 6 *B*). It also cannot be explained by Ca^{2+} release on top of an elevated end-diastolic Ca^{2+}. To the contrary, diastolic Ca^{2+} is significantly decreased (Fig. 6, *A* and *D*). The higher peak level is explained by the lower fast Ca^{2+} buffering by SERCA2b, as demonstrated in previous sections. Ca^{2+} transients are higher with the one-step SERCA schemes, but the relative difference between SERCA2a and SERCA2b in peak amplitude is preserved. The prolongation of the duration of the transient is somewhat more pronounced.

Data on the frequency dependency of the SERCA2a to SERCA2b switch at 40 μM SERCA concentration are illustrated in Fig. 6, *C* and *D*. As expected, since a lower frequency prolongs the diastolic phase of low $[Ca^{2+}]_{cyt}$, where SERCA2b is more effective, the relative performance of SERCA2b improves with decreasing frequency. This difference is accounted for by the higher loading state of the SR in the presence of SERCA2b (not shown).

To model cardiac cells of the $SERCA2^{b/b}$ mouse in which the SERCA2 concentration is reduced to ~60% of the wild-type level, SERCA2b concentrations of 40 and 24 μM were compared. The peak of the Ca^{2+} transient is only slightly shifted (Fig. 6 *C*). Diastolic levels of $[Ca^{2+}]_{cyt}$ are lower in the presence of 24 μM SERCA2b at a frequency of 6 Hz or lower, but increase at higher frequencies (Fig. 6 *D*).

Although at 8 Hz the peak amplitude of troponin-bound Ca^{2+} is slightly enhanced by an equimolar switch from SERCA2a to SERCA2b (Fig. 6, *A* and *C*), it should be noted that the pump function of the heart can be expected to be more significantly increased due to lower end-diastolic Ca^{2+} and because of the prolongation of the Ca^{2+}-bound

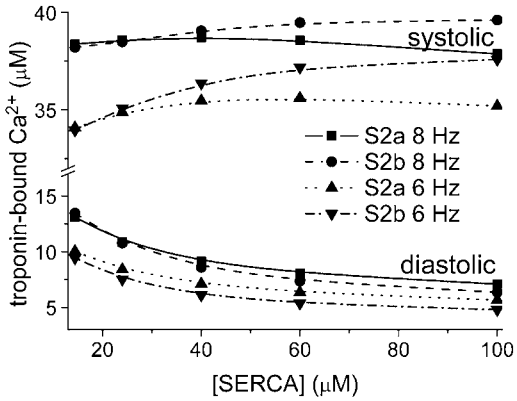

FIGURE 5 Effect of SERCA concentration on peak systolic and diastolic levels of troponin-bound Ca^{2+} at 6- and 8-Hz pacing and for SERCA2a and SERCA2b multistep kinetic schemes.

state of troponin (Fig. 6 *A*). The amount of troponin-bound Ca^{2+} integrated over time starting from its peak systolic level till it fell below 20 μM, a value well above diastolic levels (Fig. 6 *A*), was 9.4% higher in the presence of SERCA2b compared to SERCA2a, predicting a significant impact on contractility.

Simulations in stimulated conditions

Given the finding that SERCA2b, with a lower V_{max} than SERCA2a, is performing better at basal conditions, it is plausible that the lower maximal activity of SERCA2b only becomes limiting at higher Ca^{2+} concentrations. Indeed, SERCA2b became less effective during stronger activation of the contractile apparatus (Fig. 7). Stimulated conditions were implemented by increasing Ca^{2+} influx by 50% and by using a SERCA multistep model that yields Ca^{2+}-activation curves with higher affinity (S2astim and S2bstim (Table S1)), thus mimicking the effect of β-adrenergic stimulation via phosphorylation of L-type Ca^{2+} channels and phospholamban, respectively. Compared to the unstimulated condition at 8 Hz, the peak level of Ca^{2+}-bound troponin is increased by 10.6 μM with SERCA2a and 7.3 μM with SERCA2b, resulting in lower systolic levels and increased diastolic levels of Ca^{2+}-bound troponin in SERCA2b cells. Lowering SERCA2b to 60% of control further reduces the peak amplitude of Ca^{2+}-bound troponin and increases the diastolic level, which is accompanied by an increase of diastolic $[Ca^{2+}]_{cyt}$ from 62 nM (SERCA2a 60 μM, stimulated) to 79 nM (SERCA2b 36 μM, stimulated). This increase could contribute to the observed hypertrophy, whereas the reduced peak amplitude could underlie the impaired physiological stress test (11).

DISCUSSION

Ca^{2+} buffering by SERCA depends on the isoform and on the simulation model

Compared to a one-step Hill equation, representing SERCA activity by a Post-Albers kinetic scheme introduces several additional degrees of freedom in the choice of parameters, since the rate constants of each partial reaction steps are not firmly established experimentally, especially at body temperature. Thus, it is possible to change the values of

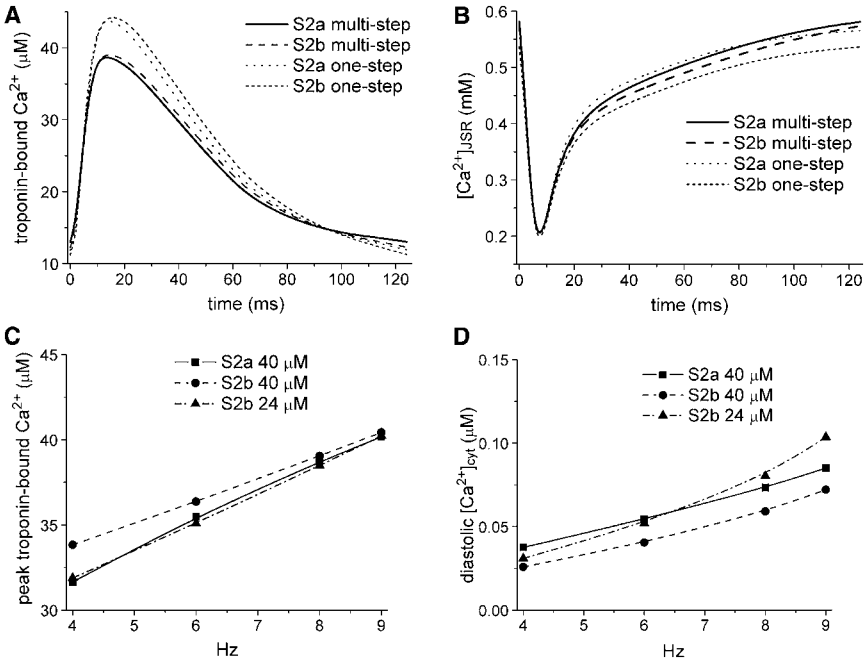

FIGURE 6 Behavior of the sarcomere model during regular pacing in the presence of SERCA2a or SERCA2b. (*A*) Time course of the change in troponin-bound Ca^{2+}. (*B*) Time dependence of the free Ca^{2+} concentration in the lumen of the JSR. (*C*) Peak values of troponin-bound Ca^{2+} during regular pacing at the indicated frequencies until a stable state is achieved. (*D*) Frequency dependence of end-diastolic $[Ca^{2+}]_{cyt}$.

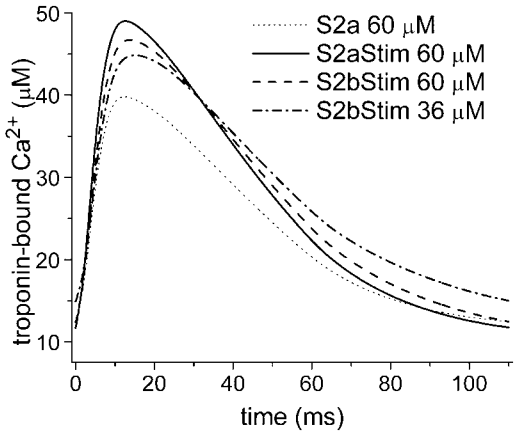

FIGURE 7 Ca^{2+} activation of troponin in stimulated conditions, using SERCA schemes S2aStim and S2bStim (Table S1) and a 50% increase of the Ca^{2+} influx.

rate constants while preserving identical Ca^{2+}-activation curves at equilibrium. The use of different sets of rate constants has implications for the extent of fast Ca^{2+} buffering, which in our scheme is moderate because of the displacement of the E1-E2 equilibrium (step 1) toward E2.

The problem of the extensive Ca^{2+} buffering by SERCA has been considered by the Baylor group in their mathematical models of Ca^{2+} transients in sarcomeres of frog and mouse fast-twitch skeletal muscle (21,22). In considering the energetic cost of a large amount of Ca^{2+} bypassing the troponin C Ca^{2+}-binding sites, these authors have chosen to incorporate additional states of SERCA1 with delayed Ca^{2+} binding. There is indeed experimental evidence for the existence of SERCA states that are dead-end complexes of Ca^{2+}-free intermediates with Mg^{2+} and/or H^+ (23–25). By choosing a slow transition rate from E1MgH toward the unliganded E1 intermediate, Ca^{2+} binding to SERCA is retarded during a sudden rise of the Ca^{2+} concentration, such as during the rising phase of the Ca^{2+} transient. We have not yet implemented these additional SERCA states for several reasons. First, there is a paucity of kinetic data on the transitions that could be involved, especially for SERCA2. Second, in the mouse heart, the implications of Ca^{2+} buffering by SERCA for the Ca^{2+} signal are expected to be less severe than in fast-twitch skeletal muscle due to the lower cardiac content of SERCA. Third, excessive SERCA1a expression obtained by gene transfer leads to impaired myocyte shortening that is adequately explained by increased Ca^{2+} buffering by SERCA (26), indicating that SERCA-related Ca^{2+} buffering indeed exists. The cost of fast Ca^{2+} binding to SERCA could be offset by buffering of the physiological effects of chronic changes of SERCA activity, for example, by oxidative damage (27–29). If SERCA levels were to respond to changes in cytosolic Ca^{2+}, the relatively small alteration of the Ca^{2+} transient with changing SERCA concentrations, at least in the high range of SERCA concentrations, suggests that the SERCA level might be sensitive to subtle signals. However, this outcome is not well supported by observations in mice with decreased SERCA2 levels carrying a null mutation in one copy of the SERCA2 gene (30), which show appreciably reduced Ca^{2+} transients despite compensatory changes in phospholamban phosphorylation and Na^+/Ca^{2+}-exchange activity. This result would better fit with a lower SERCA concentration, which, however, complicates an explanation of the $SERCA2^{b/b}$ mouse model. On the other hand, rapid cardiac-specific ablation of the SERCA2 gene is initially well tolerated (31).

The difference in pump activity between SERCA2a and SERCA2b depends mainly on the Ca^{2+} affinity

SERCA2a has a twofold-higher catalytic turnover rate than SERCA2b, but only half the Ca^{2+} affinity of SERCA2b. Assuming that kinetic differences in Ca^{2+} transport have prompted the selective expression of SERCA2a over SERCA2b in cardiac cells, it would seem that the faster maximal turnover of SERCA2a is more appropriate for heart function than the higher Ca^{2+} affinity of SERCA2b, i.e., the higher Ca^{2+} affinity of SERCA2b appears unlikely to compensate for its lower turnover rate. However, several findings on the $SERCA2^{b/b}$ mouse appear to contradict this interpretation. In these gene-modified animals, an apparently compensatory downregulation of cardiac SERCA2 levels and an increased inhibition of phospholamban are seen. Both of these alterations result in less pump activity at low cytosolic Ca^{2+} levels, suggesting that it is rather the high Ca^{2+} affinity of SERCA2b that is not well tolerated. The simulations presented here support this hypothesis for the mouse heart in unstimulated conditions. The better performance of SERCA2b under low workload is seen with both the one-step and multistep SERCA representations. This effect is explained in part by the lower competition of SERCA2b with the binding sites on troponin C, due to the lower extent of fast Ca^{2+} buffering. The contribution of SERCA buffering explains why the relative performance of SERCA2b increases with increasing SERCA concentrations entered into the model (Fig. 5). With our current knowledge about the kinetic properties of SERCA2b and the compensatory changes in the $SERCA2^{b/b}$ mouse, the downregulation of SERCA in the transgenic animals can best be explained if the normal SERCA level is ~40 μM or higher. This concentration is well within the range compatible with experimental observations (14).

Limitations of the study

The simulations presented here are the result of a particular choice of values for the model parameters, several of which may have significant quantitative effects. In particular, the

value accepted for the degree of saturation of troponin with Ca^{2+} during systole in the unstimulated heart, and the relative affinity of troponin C and SERCA for Ca^{2+}, can be expected to be critical parameters affecting the relative over-all transport capacity of the SERCA isoforms. As can be expected intuitively, and also confirmed by the computer simulations (not shown), relative SERCA2b performance will increase with increasing Ca^{2+} affinity of the contractile filaments because of the activation of the contractile apparatus at lower average Ca^{2+} concentrations. All simulations in basal conditions shown in this article apply to the condition of approximately equal Ca^{2+} affinities of SERCA2a and troponin C during systole. Another important constraint is the accepted systolic and diastolic levels of troponin-bound Ca^{2+}.

Besides these troponin-related parameters, the concentration of SERCA and the characteristics of the Ca^{2+} efflux determine the results of the model. Because of the large contribution of Ca^{2+} buffering by SERCA and the different buffering characteristics of SERCA2a and SERCA2b, the SERCA concentration codetermines the outcome of the isoform replacement. The SERCA concentration required to sustain a specific amplitude of the Ca^{2+} signal is also determined by the maximal turnover rate. This value is not firmly established, in particular at body temperature. Furthermore, as expected intuitively, the relative effectiveness of SERCA2b increases with increasing rate of Ca^{2+} efflux in the low Ca^{2+} range relative to the higher Ca^{2+} concentrations (data not shown). When more quantitative information on the in vivo parameters is obtained, the simulations and their outcome may have to be adjusted accordingly.

Qualitatively, the better performance of SERCA2b, taking into account the known kinetic characteristics of this isoform, is a robust result of the simulations. It should also be taken into account that in the mutant mice, normal force can be maintained with lower Ca^{2+} transients because of the hypertrophied state of the heart (9). However, the existence of additional, yet unknown differences between SERCA2a and SERCA2b and unidentified compensatory or other changes in the transgenic animals may contribute as well to the down-regulation of SERCA in the $SERCA2^{b/b}$ mouse.

Modeling supports a predominant role for SERCA's Ca^{2+} affinity in basal conditions

Computer modeling has demonstrated that the major effects of the SERCA2a-to-SERCA2b switch result in a slightly higher peak level of the Ca^{2+} transient, a longer period of activation of the filaments, and a lower end-diastolic Ca^{2+} concentration in the unstimulated heart. This effect increases with decreasing contraction strength, as shown by the frequency dependence (Fig. 6, *C* and *D*) and by the effects in stimulated conditions (Fig. 7). $[Ca^{2+}]_{cyt}$ is on average lower in basal conditions than in the stimulated heart, shifting the relative importance of the difference in V_{max} and $K_{0.5}$ of SERCA2a and SERCA2b toward the Ca^{2+} affinity. However, since the gain of function of replacing SERCA2a by SERCA2b is not really impressive, it remains a surprising observation that in the $SERCA2^{b/b}$ mouse, SERCA levels are drastically reduced to ~60% of wild-type, moreover in combination with an up-regulation of inhibitory phospholamban levels. The simulations presented here do not quantitatively account for this strong reduction. At face value, the simulations indicate that a factor contributing to the adjustment of the SERCA levels could be the diastolic Ca^{2+} concentration in basal conditions. Although normal systolic Ca^{2+} saturation of troponin C is slightly lower with SERCA2b at 60% of normal levels (Fig. 6 *C*), diastolic Ca^{2+} is below normal, at least at frequencies of 6 Hz or lower (Fig. 6 *D*). In vivo, it is likely that diastolic Ca^{2+} ends up at a higher level because of the additional upregulation of the inhibition of SERCA activity by phospholamban.

In stimulated conditions, the over-all Ca^{2+}-transport capacity of SERCA2b relative to that of SERCA2a is strongly reduced. This result is in line with experimental observations on the $SERCA2^{b/b}$ mouse, which show that the Ca^{2+} uptake by the SR is impaired at higher Ca^{2+} loads only (10). SERCA2a might thus be a better compromise between performance both in basal conditions and during β-adrenergic stress. The model predicts an elevated diastolic Ca^{2+} in $SERCA2^{b/b}$ myocytes in stressed conditions, which may be a contributing factor to the observed hypertrophy through activation of calcineurin.

SUPPORTING MATERIAL

Three figures and three tables are available at http://www.biophysj.org/biophysj/supplemental/S0006-3495(11)00107-X.

This research was financed by the Research Foundation-Flanders (Fonds Wetenschappelijk Onderzoek-Vlaanderen, G.0646.08) and by the Interuniversity Attraction Poles Program P6/28 of the Belgian State, Federal Office for Scientific Technical and Cultural Affairs.

REFERENCES

1. Bers, D. M. 2002. Cardiac excitation-contraction coupling. *Nature.* 415:198–205.
2. MacLennan, D. H., and E. G. Kranias. 2003. Phospholamban: a crucial regulator of cardiac contractility. *Nat. Rev. Mol. Cell Biol.* 4:566–577.
3. Bers, D. M. 2001. Excitation-Contraction Coupling and Cardiac Contractile Force. Kluwer Academic, Norwell, MA.
4. Dash, R., V. Kadambi, …, E. G. Kranias. 2001. Interactions between phospholamban and β-adrenergic drive may lead to cardiomyopathy and early mortality. *Circulation.* 103:889–896.
5. Schmitt, J. P., M. Kamisago, …, C. E. Seidman. 2003. Dilated cardiomyopathy and heart failure caused by a mutation in phospholamban. *Science.* 299:1410–1413.
6. Vangheluwe, P., L. Raeymaekers, …, F. Wuytack. 2005. Modulating sarco(endo)plasmic reticulum Ca^{2+} ATPase 2 (SERCA2) activity: cell biological implications. *Cell Calcium.* 38:291–302.

7. Dode, L., J. P. Andersen, …, A. Hovnanian. 2003. Dissection of the functional differences between sarco(endo)plasmic reticulum Ca^{2+}-ATPase (SERCA) 1 and 2 isoforms and characterization of Darier disease (SERCA2) mutants by steady-state and transient kinetic analyses. *J. Biol. Chem.* 278:47877–47889.
8. Verboomen, H., F. Wuytack, …, R. Casteels. 1992. Functional difference between SERCA2a and SERCA2b Ca^{2+} pumps and their modulation by phospholamban. *Biochem. J.* 286:591–595.
9. Ver Heyen, M., S. Heymans, …, F. Wuytack. 2001. Replacement of the muscle-specific sarcoplasmic reticulum Ca^{2+}-ATPase isoform SERCA2a by the nonmuscle SERCA2b homologue causes mild concentric hypertrophy and impairs contraction-relaxation of the heart. *Circ. Res.* 89:838–846.
10. Antoons, G., M. Ver Heyen, …, K. R. Sipido. 2003. Ca^{2+} uptake by the sarcoplasmic reticulum in ventricular myocytes of the $SERCA2^{b/b}$ mouse is impaired at higher Ca^{2+} loads only. *Circ. Res.* 92:881–887.
11. Vangheluwe, P., M. Tjwa, …, F. Wuytack. 2006. A SERCA2 pump with an increased Ca^{2+} affinity can lead to severe cardiac hypertrophy, stress intolerance and reduced life span. *J. Mol. Cell. Cardiol.* 41: 308–317.
12. Vangheluwe, P., M. Schuermans, …, F. Wuytack. 2007. Tight interplay between the Ca^{2+} affinity of the cardiac SERCA2 Ca^{2+} pump and the SERCA2 expression level. *Cell Calcium.* 42:281–289.
13. Vandecaetsbeek, I., M. Trekels, …, P. Vangheluwe. 2009. Structural basis for the high Ca^{2+} affinity of the ubiquitous SERCA2b Ca^{2+} pump. *Proc. Natl. Acad. Sci. USA.* 106:18533–18538.
14. Hove-Madsen, L., and D. M. Bers. 1993. Sarcoplasmic reticulum Ca^{2+} uptake and thapsigargin sensitivity in permeabilized rabbit and rat ventricular myocytes. *Circ. Res.* 73:820–828.
15. Edman, K. A. 1996. Fatigue vs. shortening-induced deactivation in striated muscle. *Acta Physiol. Scand.* 156:183–192.
16. Hinken, A. C., and R. J. Solaro. 2007. A dominant role of cardiac molecular motors in the intrinsic regulation of ventricular ejection and relaxation. *Physiology (Bethesda).* 22:73–80.
17. Cannell, M. B., and D. G. Allen. 1984. Model of calcium movements during activation in the sarcomere of frog skeletal muscle. *Biophys. J.* 45:913–925.
18. Baylor, S. M., and S. Hollingworth. 1998. Model of sarcomeric Ca^{2+} movements, including ATP Ca^{2+} binding and diffusion, during activation of frog skeletal muscle. *J. Gen. Physiol.* 112:297–316.
19. Shannon, T. R., K. S. Ginsburg, and D. M. Bers. 2000. Potentiation of fractional sarcoplasmic reticulum calcium release by total and free intra-sarcoplasmic reticulum calcium concentration. *Biophys. J.* 78:334–343.
20. Isenberg, G., E. F. Etter, …, F. S. Fay. 1996. Intrasarcomere [Ca^{2+}] gradients in ventricular myocytes revealed by high speed digital imaging microscopy. *Proc. Natl. Acad. Sci. USA.* 93:5413–5418.
21. Baylor, S. M., and S. Hollingworth. 2007. Simulation of Ca^{2+} movements within the sarcomere of fast-twitch mouse fibers stimulated by action potentials. *J. Gen. Physiol.* 130:283–302.
22. Hollingworth, S., W. K. Chandler, and S. M. Baylor. 2006. Effects of tetracaine on voltage-activated calcium sparks in frog intact skeletal muscle fibers. *J. Gen. Physiol.* 127:291–307.
23. Inesi, G., D. Lewis, …, L. de Meis. 2008. Conformational fluctuations of the Ca^{2+}-ATPase in the native membrane environment. Effects of pH, temperature, catalytic substrates, and thapsigargin. *J. Biol. Chem.* 283:1189–1196.
24. Peinelt, C., and H. J. Apell. 2002. Kinetics of the Ca^{2+}, H^{+}, and Mg^{2+} interaction with the ion-binding sites of the SR Ca-ATPase. *Biophys. J.* 82:170–181.
25. Zafar, S., A. Hussain, …, G. Inesi. 2008. Specificity of ligand binding to transport sites: Ca^{2+} binding to the Ca^{2+} transport ATPase and its dependence on H^{+} and Mg^{2+}. *Arch. Biochem. Biophys.* 476:87–94.
26. Teucher, N., J. Prestle, …, G. L. Smith. 2004. Excessive sarcoplasmic/endoplasmic reticulum Ca^{2+}-ATPase expression causes increased sarcoplasmic reticulum Ca^{2+} uptake but decreases myocyte shortening. *Circulation.* 110:3553–3559.
27. Grover, A. K., S. E. Samson, and V. P. Fomin. 1992. Peroxide inactivates calcium pumps in pig coronary artery. *Am. J. Physiol. Heart Circ. Physiol.* 263:H537–H543.
28. Suzuki, Y. J., and G. D. Ford. 1991. Inhibition of Ca^{2+}-ATPase of vascular smooth muscle sarcoplasmic reticulum by reactive oxygen intermediates. *Am. J. Physiol. Heart Circ. Physiol.* 261:H568–H574.
29. Xu, K. Y., J. L. Zweier, and L. C. Becker. 1997. Hydroxyl radical inhibits sarcoplasmic reticulum Ca^{2+}-ATPase function by direct attack on the ATP binding site. *Circ. Res.* 80:76–81.
30. Ji, Y., M. J. Lalli, …, M. Periasamy. 2000. Disruption of a single copy of the SERCA2 gene results in altered Ca^{2+} homeostasis and cardiomyocyte function. *J. Biol. Chem.* 275:38073–38080.
31. Andersson, K. B., J. A. Birkeland, …, G. Christensen. 2009. Moderate heart dysfunction in mice with inducible cardiomyocyte-specific excision of the Serca2 gene. *J. Mol. Cell. Cardiol.* 47:180–187.